JOURNAL OF GEOPHYSICAL RESEARCH, VOL. 105, NO. D21, PAGES 26,519–26,530, NOVEMBER 16, 2000

The seasonal cycle of water vapor and saturation vapor mixing ratio in the extratropical lowermost stratosphere

Liwen L. Pan,[1] Eric J. Hintsa,[2,3] Elizabeth M. Stone,[4,5] Elliot M. Weinstock,[2] and William J. Randel[1]

Abstract. Both in situ measurements and satellite remote sensing data show that water vapor in the extratropical lowermost stratosphere has a pronounced seasonal cycle, with a maximum in summer. In this paper we show that the seasonal cycles derived from satellite measurements by the Stratospheric Aerosol and Gas Experiment (SAGE) II and the Microwave Limb Sounder (MLS) and ER-2 aircraft measurements are in reasonable agreement when compared using potential vorticity (PV) and potential temperature (θ) binned monthly averages. The annual means and amplitudes of the water vapor seasonal cycle are derived from the SAGE II data for 320-360 K and 2-7 PV units (covering latitudes near and poleward of the tropopause). The high moisture content and the summer maxima indicate that the effect of transport from the troposphere across the extratropical tropopause can be seen in nearly the entire range examined and is more significant in the lower PV–θ bins. We further investigate mechanisms that control the amount and seasonal cycle of water vapor in the lowermost stratosphere. One important issue is whether local temperature near the extratropical tropopause limits isentropic transport of water vapor into the lowermost stratosphere, similar to the freeze-out of water vapor crossing the tropical tropopause. A quantitative comparison of saturation vapor mixing ratios (derived from National Centers for Environmental Prediction temperature analyses) with the water vapor measurements shows that the amount of water vapor near the extratropical tropopause is substantially lower than that given by saturation over ice. This demonstrates that local temperature effects do not set the upper limit of water vapor in this region. Analyses using ER-2 measurements confirm that although saturation and supersaturation do occur, on average, air near the extratropical tropopause is undersaturated. The seasonal cycle of the fraction of the overworld air in the lowermost stratosphere is inferred using the water vapor and saturation vapor mixing ratio climatology.

1. Introduction

The distribution and variability of water vapor in the lower stratosphere and upper troposphere are of importance to the Earth's radiative balance, to ozone chemistry, and to the understanding and quantification of stratosphere-troposphere exchange (STE). In this paper we present a quantitative description of the water vapor seasonal cycle in the lowermost stratosphere, the region of the stratosphere between the extratropical tropopause and 380 K [*Holton et al.*, 1995], based on long records of satellite and aircraft data. We furthermore use temperature observations to quantify the degree of saturation and its seasonal variation from the different data sources. Finally, we use the water vapor climatology in an idealized budget analysis to constrain monthly mass transport in the lowermost stratosphere.

Analyses using both in situ measured and remotely sensed data have shown that water vapor in the lowermost stratosphere has a pronounced seasonal cycle. The maximum occurs in the summer season, and the minimum occurs in winter [*Foot*, 1984; *Dessler et al.*, 1995; *Pan et al.*, 1997; *Stone et al.*, 2000]. In particular, the seasonal cycle and hemispheric differences of water vapor in the lowermost stratosphere have been given by *Pan et al.* [1997] using global satellite data. There are, however, several limitations in the analyses of *Pan et al.* [1997]. First, the derived seasonal cycle is associated with a large uncertainty, because the data are from a region that is near the margin of the instrument sensitivity. Second, the derived monthly means were potentially influenced by the variation of the tropopause height and by the latitudinal range of the sampling. Third, the seasonal cycles were given as averages of all selected lowermost stratospheric data on a set of isentropes. The variation of water vapor mixing ratio on the same isentrope inside the stratosphere was not resolved. These issues are directly addressed in section 3 of the present paper.

To address the first issue, i.e., the reliability of satellite climatologies in this region, we have compared water vapor measurements derived from two satellite instruments, Stratospheric Aerosol and Gas Experiment (SAGE) II and the Microwave Limb Sounder (MLS), with in situ measurements from the Stratospheric TRacers of Atmospheric Transport

[1]National Center for Atmospheric Research, Boulder, Colorado.
[2]Department of Chemistry and Biological Chemistry, Harvard University, Cambridge, Massachusetts.
[3]Now at Department of Marine Chemistry and Geochemistry, Woods Hole Oceanographic Institution, Woods Hole, Massachusetts.
[4]Jet Propulsion Laboratory, California Institute of Technology, Pasadena.
[5]Now at Bay Area Environmental Research Institute, NASA Ames Research Center, Moffett Field, California.

Paper number 2000JD900401
0148-0227/00/2000JD900401$09.00

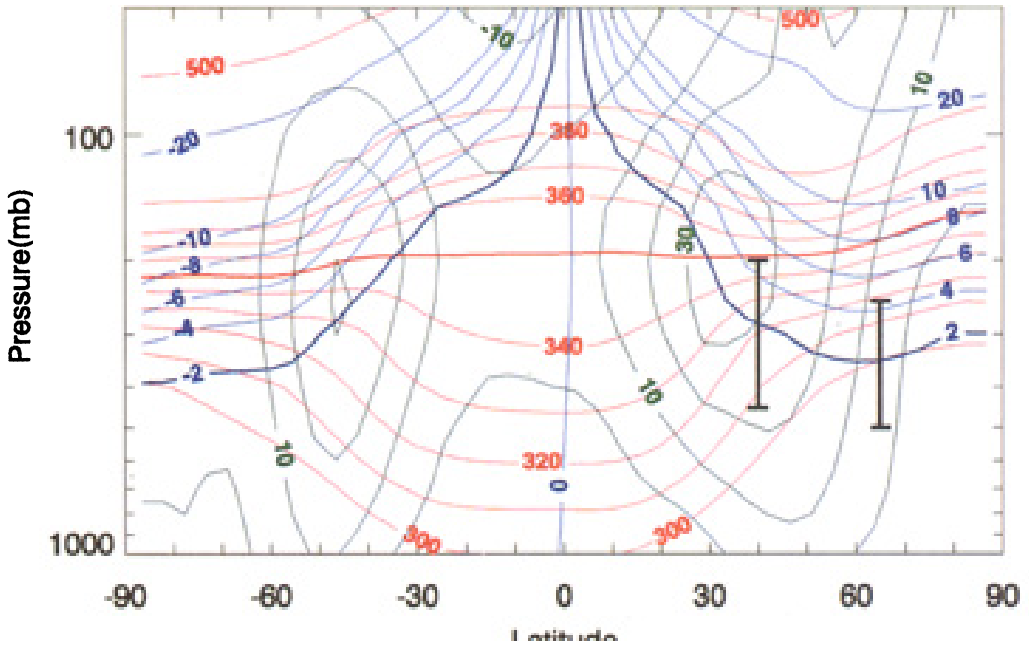

Plate 1. Monthly mean potential temperature (red), potential vorticity (blue), and zonal wind (green) in pressure-latitude coordinates for January 1990, derived from the National Centers for Environmental Prediction (NCEP) Climate Prediction Center stratospheric analyses data. The dynamical tropopause is represented by the 380-K contour in the tropics and the 2 PVU (PVU is potential vorticity unit) contour in the extratropics. The PV=2 and θ=350 K contours are highlighted by bold lines. The vertical bars I mark the latitudinal positions of the ER-2 measurements near the extratropical tropopause.

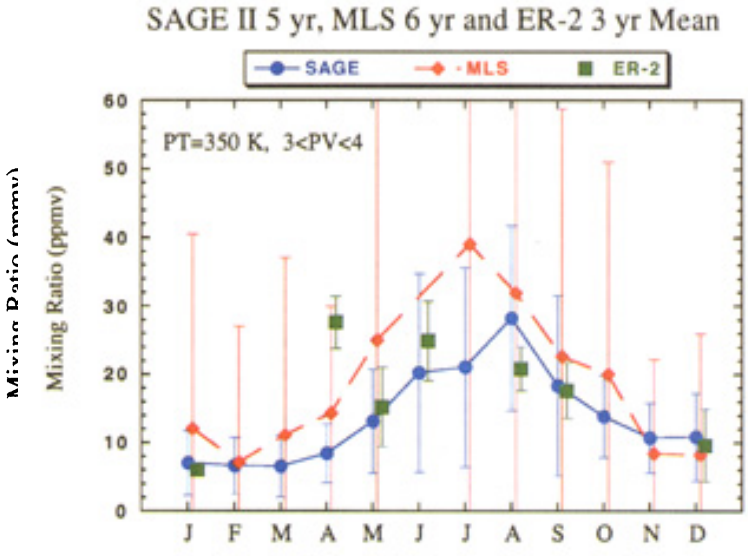

Plate 2. Comparisons of middle world water vapor from Stratospheric Aerosol and Gas Experiment Microwave Limb Sounder (SAGE) II, Microwave Limb Sounder (MLS), and aircraft in situ measurements for the 350-K isentrope (±5 K layer) and 3-4 PVU. The SAGE II points are 5-year means from all data points in the range 1986-1990. The MLS points are 6-year means (1992-1997). The in situ data are mean values for all data points in this range in the Stratospheric TRacers of Atmospheric Transport/Photochemistry of Ozone Loss in the Arctic Regions In Summer (STRAT/POLARIS) missions (1995-1997), with the error bar indicating the root-mean-square deviation from the mean.

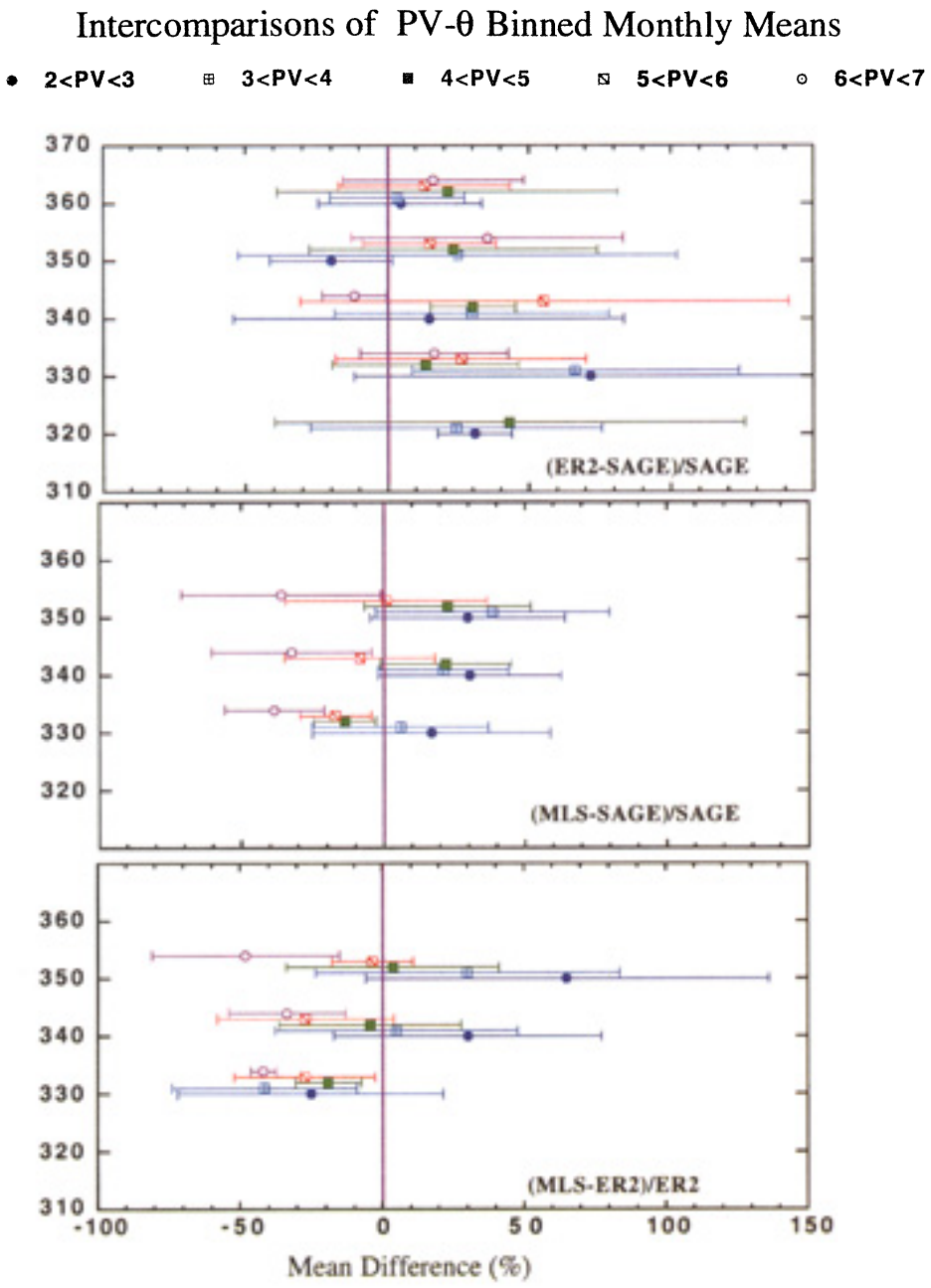

Plate 3. Intercomparisons of monthly means derived from SAGE II, MLS, and ER-2 for the lowermost stratospheric PV-θ bins. The symbols represent the average difference of the monthly means, as shown in Plate 2, over the seasonal cycle. The error bars indicate the standard deviation from the mean. The top panel shows the percentage difference between ER-2 and SAGE; the middle panel is between MLS and SAGE; and the bottom panel is between MLS and ER2.

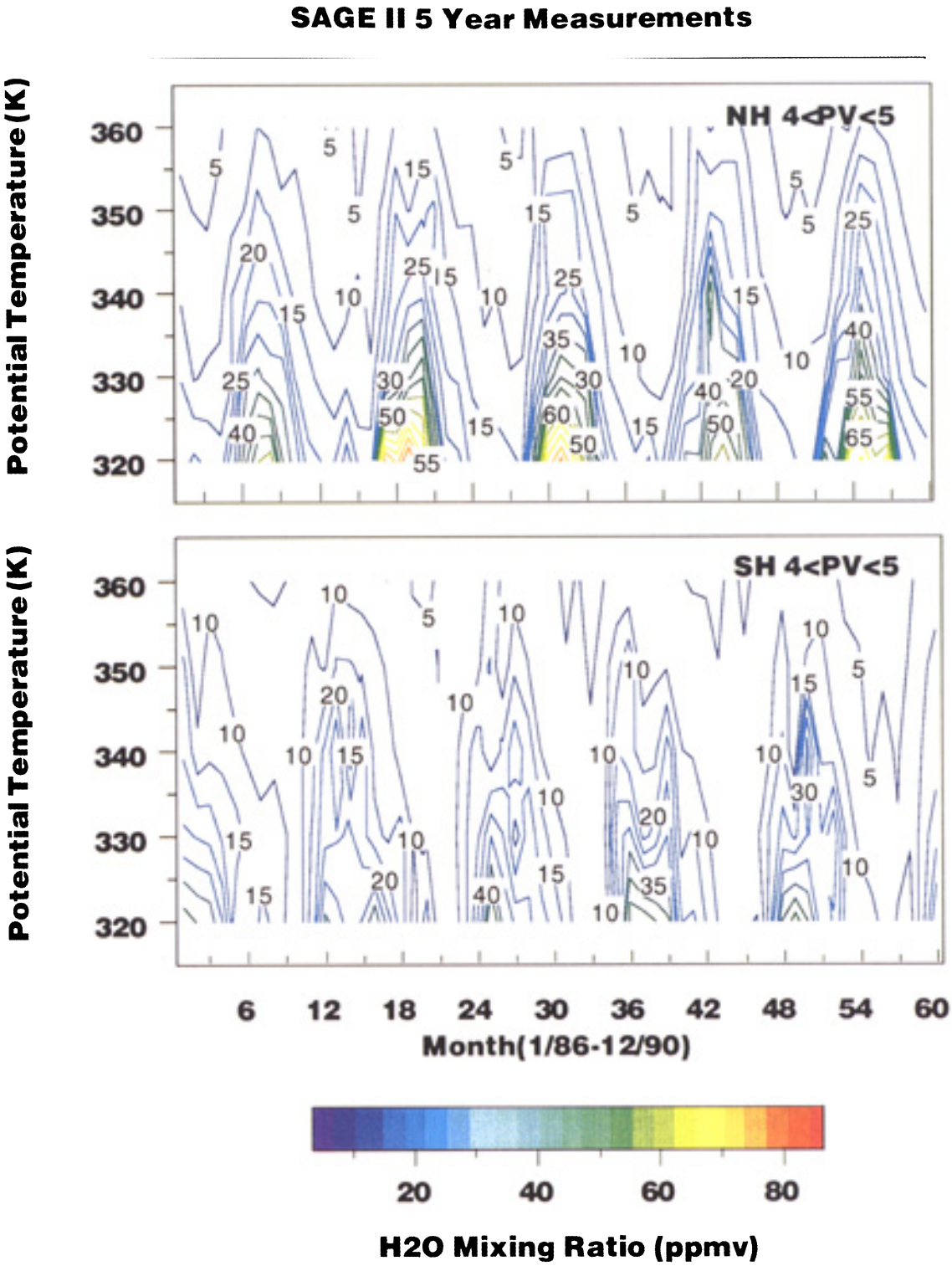

Plate 4. Five-year (January 1986-December 1990) SAGE II water monthly mean values for the 4-5 PVU bin and 320-360 K potential temperature (10 K layers). The contours are drawn in 5-ppmv intervals. The missing values (Northern Hemisphere 320 K in July and Southern Hemisphere in January) are filled by a fit to the seasonal cycle. Figure 2. Annual mean, January and July monthly mean as a function of PV for 330-360 K derived from the 5-year (January 1986-December 1990) SAGE II measurements for the 2-7 PVU. The data are binned in 1-PVU intervals. PV values shown for each panel are the lower boundary of each PV bin. Note the variation of scales for the vertical coordinates, selected to best display the range of seasonal variations.

(STRAT) and the Photochemistry of Ozone Loss in the Arctic Region In Summer (POLARIS) missions. Since these measurements were taken in different years with different sampling strategies, we attempt to put the data sets on a common footing using the dynamically based coordinates of potential vorticity (PV) and potential temperature (θ) [*Hoskins*, 1991]. The use of PV-θ coordinates not only facilitates comparisons of data among dynamically equivalent air parcels, but also helps to separate the seasonal variation of water vapor from the variation of tropopause height. PV values are useful indications of how "deep" the air parcels are in the stratosphere, since the dynamical tropopause is usually defined by PV. Using Ertel's PV, PV values of 2-3 PV units, or PVU (1 PVU= $1x10^{-6}$ m^2 K s^{-1} kg^{-1}), or higher are associated with stratospheric air [*Holton et al.*, 1995]. Using PV based averages, we also quantify the spatial variation of water vapor inside the lowermost stratosphere.

In addition to these aforementioned issues, we investigate the effect of temperature on the transport of water vapor in the middle world. The lowermost stratosphere is composed of a mixture of air from the upper troposphere, transported by STE processes across the extratropical tropopause, and air from the overworld, transported by the large-scale Brewer-Dobson circulation [*Holton et al.*, 1995, and references therein]. The seasonal cycle in water vapor is a result of these two competing processes [*Dessler et al.*, 1995; *Pan et al.*, 1997; *Hintsa et al.*, 1998]. The seasonal cycle of the large-scale downward circulation and the boundary conditions for water vapor transport from the overworld are reasonably well known. In contrast, both the boundary conditions and the seasonal variability of transport across the extratropical tropopause are poorly known. In this paper we compare saturation mixing ratios, derived using temperature data, with water vapor mixing ratios near the extratropical tropopause, as a step toward understanding the boundary conditions of this transport process.

The objectives of this paper are twofold. The first is to quantify the seasonal cycle of water vapor in the lowermost stratosphere given the currently available satellite and in situ data. The second is to examine the effect of temperature as a limiting factor on water vapor in this region. Combining the global satellite data with the more accurate aircraft in situ data in this analysis not only serves to validate the results, but more important, it also allows us to address the outstanding issues using the combined strengths of these two types of measurements.

2. Descriptions of Data

Water vapor data used in this analysis are from two satellite instruments, SAGE II and MLS, and an aircraft in situ instrument, the Harvard Lyman-α hygrometer, on board the ER-2 aircraft during the STRAT and POLARIS missions. Global temperature data from the National Centers for Environmental Prediction (NCEP) are used in the saturation mixing ratio analysis for the satellite data. Temperature measurements from the Meteorological Measurement System (MMS) on the ER-2 are used with the coincident ER-2 water vapor data to derive relative humidity values.

SAGE II is a satellite solar occultation experiment [*McCormick*, 1987; *McCormick et al.*, 1993]. More than 5 years (January 1986 to May 1991) of water vapor mixing ratio data have been produced by the experiment [*Chiou et al.*, 1997]. SAGE II is still taking data, and the post-Pinatubo data will be available in the future. Retrieval analyses and validation studies show that SAGE II water vapor data, in the region of our study, have an uncertainty level of the order of 20% [*Chu et al.*, 1993; *Rind et al.*, 1993]. The water vapor profiles are retrieved for clear conditions with a 1-km vertical resolution. Fifteen sunrise and 15 sunset measurements are made each day around the same latitude. A latitude range of approximately 70°S-70°N is covered in each season.

The MLS measurement technique is described by *Waters* [1993]. The retrieval and validation of the upper troposphere humidity (UTH) product is presented by W. Read et al. (manuscript in preparation, 2000). The MLS instrument measures ~1300 profiles daily, covering the globe from 80 degrees latitude in one hemisphere to 34° latitude in the other, alternating every ~36 days. The UTH data are available on four pressure levels (464, 316, 215, and 147 hPa) with 100 × 200 km horizontal resolution and a vertical resolution of 2.7-4 km, depending on the pressure and moisture content of the atmosphere. The instrument is less sensitive for measuring low mixing ratios (~10 ppmv or lower). The technique allows measurement in the presence of cirrus clouds. The monthly means are compiled for September 1991 to June 1997, with nonhomogenous temporal sampling. After the first 3 years, UARS power limitations and MLS scan problems resulted in a decreased observation schedule.

In situ water vapor data used in this analysis are from the Harvard Lyman-α hygrometer [*Weinstock et al.*, 1994], which was flown on board the NASA ER-2 aircraft. During the STRAT and POLARIS missions, water vapor was measured on approximately 70 flights over a latitude range from 2°S to 90°N. Data were obtained in all seasons from the midtroposphere to 21 km. However, most of the data in the lowermost stratosphere are concentrated in latitude bands over 35-40°N and 64°-67°N, near two of the aircraft deployment locations, NASA Ames Research Center (37°N, 122°W) and Fort Wainwright, Fairbanks, Alaska (65°N, 148°W). Water vapor data are reported every 4 s and have been shown to have an accuracy of ±5% [*Hintsa et al.*, 1999]. For this study, all ER-2 data have been averaged to 10 s, leading to a horizontal resolution of ~2 km and a vertical resolution of 0.1-0.2 km.

Coincident temperature and pressure data on the ER-2 were obtained from the MMS [*Scott et al.*, 1990], with accuracies better than 1 K and ±0.3 mbar, respectively. Tropopause heights were determined for each flight from combinations of MMS and remote sensing microwave temperature profiler (MTP) [*Denning et al.*, 1989] data, using the standard World Meteorological Organization (WMO) definition for the thermal tropopause. Typical uncertainties in thermal tropopause heights are ±0.1-0.3 km.

Coincident PV values for the SAGE II and MLS measurements are determined by spatially interpolating daily PV values computed from NCEP Climate Prediction Center stratospheric analyses data. For the ER-2 data the PV values are computed from the Goddard data assimilation model output, which is produced for every 6-hour period on a 2°×2.5° latitude-longitude grid at standard pressure levels.

3. Seasonal Cycle of Water Vapor

To assess the level of qualitative and quantitative agreement in derived seasonal cycles from the three data sets, we have computed monthly average water vapor mixing ratios from SAGE

II, MLS, and Lyman-α data using the dynamically based coordinates of PV and θ. PV-θ binned monthly averages are compared for the PV range 2-7 PVU and the θ range 320-360 K. In this section we first illustrate the spatial location and the seasonal variation of this PV-θ range in pressure-latitude coordinates, using Plate 1 and Figure 1. Second, an example showing the qualitative agreement in the derived seasonal cycle between the three data sets is given in Plate 2. The differences between the PV-based climatologies are quantified and summarized in Plate 3. Last, a quantitative description of the water vapor seasonal cycle in this PV-θ range derived from the SAGE II data is given in Plate 4 and Figure 2.

Plate 1 displays PV, θ, and zonal wind in pressure-latitude coordinates for monthly mean conditions in January. This plate illustrates the position of the region we study relative to the tropopause and the wind maxima. In addition, the latitude positions of ER-2 measurements in the extratropical lowermost stratosphere are marked on this plate. A range of PV values has been suggested to define the dynamical tropopause in the extratropics [*Hoerling et al.*, 1991; *Holton et al.*, 1995]. In this analysis we consider the 2-3 PVU bin as the tropopause bin, following *Holton et al.* [1995]. One relevant detail is that the latitude position and pressure level of the intersections of the tropopause with each isentrope vary with season. For example, the 350-K isentrope intersects the extratropical tropopause around the 200-mbar pressure level, near 35° latitude in the summer hemisphere, 30° latitude in the winter hemisphere, and close to the center of the subtropical jet in both hemispheres. Similarly, the latitude positions and pressure levels of each PV-θ bin also change with season.

To illustrate the seasonal variation of the PV-θ range of this analysis on a given isentrope, Figure 1 shows the equivalent latitude for several PV values during 1 year, using the 330-K isentrope as an example. The equivalent latitude for a PV value is the latitude that encloses the same hemispheric area as that PV contour. This figure shows that the stratospheric portion of the hemispheric area (PV>2 PVU) for the isentrope varies from a maximum in winter to a minimum in summer. The latitudinal position of the tropopause, as indicated by the 2-PVU contour in Figure 1, varies from ~35° to 60° for the Northern Hemisphere (NH) and from 30° to 50° for the Southern Hemisphere (SH). The seasonal variations are qualitatively the same for other isentropes in the lowermost stratosphere, but the equivalent latitudes for these PV values are lower for higher isentropes, as can be inferred from Plate 1. Figure 1 illustrates an important difference between PV-based averages and the latitudinal zonal means: Both the seasonal cycle of the atmospheric constituents and the seasonal variation of the extratropical tropopause position will contribute to the latitudinal zonal mean, but the latter is removed in a PV-based average.

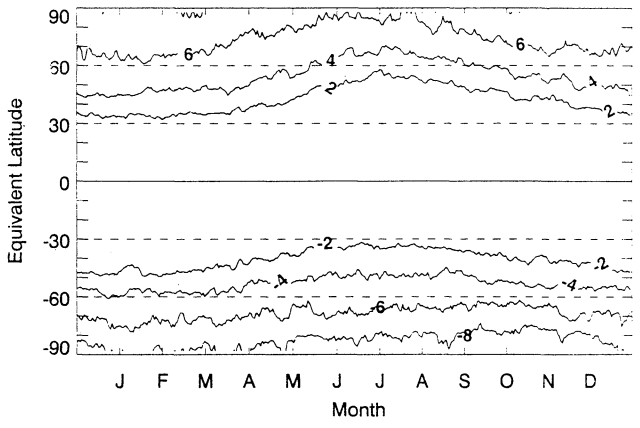

Figure 1. Daily equivalent latitude of 2, 4, 6, and 8 PVU for the 330 K-isentrope. The contours are computed using NCEP data for 1996.

Plate 2 gives an example of the water vapor seasonal climatology derived from the three data sources using the dynamical coordinates. The monthly averages are computed using all data points that fall into the given PV (in 1-PVU intervals) and θ (in 10-K layers) ranges. The compiled climatologies include 5 years of SAGE II data (January 1986 to December 1990), 6 years of MLS data (September 1991 to June 1997), and 3 years of ER-2 data (selected months for 1995-1997), with their space-time sampling as described above. Plate 2 shows the comparison for the 350 (±5) K, 3-4 PVU bin (near the tropopause). As the example shows, the mean values and the variances (expressed as the standard deviation in the plate) from MLS are typically larger than those from SAGE II in the wetter seasons. This is consistent with the fact that MLS has a 3-km vertical resolution, as compared with the 1-km vertical resolution of SAGE II. Since the water vapor mixing ratio has a steep vertical gradient in this region, MLS results (representative of a 3-km-thick layer) may show a wet bias (or dry bias; see discussion of Plate 3) in comparison with the SAGE data. This depends on the shape of the weighting function and its peak position relative to the nominal pressure of the layer. Another possible factor that contributes to the positive MLS-SAGE difference in the wetter season is that the SAGE data are only produced for clear conditions, while MLS data include observations under cloudy conditions.

In comparing the satellite average with that from the ER-2 data, it is important to note that the ER-2 data have a much smaller number of samples (total ~70 flights) and the measurements were taken over a narrow longitudinal range (~120°-150°W), compared with the satellite data. The monthly average produced is more likely to be subject to longitudinal variations and the timing of the sampling, although this is minimized in our PV-θ analyses.

Plate 3 summarizes the differences in derived monthly means over the seasonal cycles between the three sets of measurements as functions of PV and θ. In this plate, the symbols display the mean percentage difference over each derived seasonal cycle for a PV-θ bin between ER-2 and SAGE II data (top panel), MLS and SAGE II (middle panel), and MLS and ER-2 (bottom panel). The error bars give the standard deviation (σ) of the difference. For the MLS-SAGE II comparisons the symbols approximate the difference in derived annual mean for each bin, since both MLS and SAGE II sample nearly the full seasonal cycle. In the cases of comparisons with the ER-2 data, the means are computed from months with both ER-2 and SAGE (or MLS) data, as illustrated in Plate 2.

As indicated in the top panel of Plate 3, the average ER-2-SAGE differences are nearly always positive with a couple of exceptions. The overall average difference for the bins included in the plate is 24%, and there is no strong dependence on PV or θ. The middle panel of a Plate 3 shows that average MLS-SAGE differences vary nearly monotonically from low to high PV bins. The lowest PV bin (2-3 PVU) has the highest positive difference, on average (26%), while the highest PV bin (6-7 PVU) has a negative difference (-35%). The SAGE-MLS comparisons are

consistent with the difference in the vertical resolution of the data sets and the limited sensitivity of MLS to low mixing ratios in the highest PV bins. Plate 3 suggests that MLS tends to report lower mixing ratios, as compared with SAGE and ER-2 data, in measuring drier air, i.e., where the water vapor mixing ratio is less than 10 ppmv. The overall pattern of the MLS-ER-2 comparison, shown in the bottom panel of Plate 3, is similar to the MLS-SAGE comparison, but the overall differences are slightly more negative, which is consistent with the general positive bias of the ER-2-SAGE comparison. We have made similar comparisons of the three data sets for the individual winter and summer seasons (not shown). The overall patterns of average differences in these two seasons are very similar to that shown in Plate 3.

Plates 2 and 3 show that despite the differences in sampling, the derived monthly means and seasonal cycles from the three data sets are in reasonable agreement in this region of the atmosphere. The variation of MLS-SAGE (ER-2) differences with PV bin are consistent with the sampling differences and the limitations of the data (MLS UTH is designed to report upper tropospheric water vapor and is less sensitive in reporting very dry air). Although there are mean biases of order 20% between SAGE and ER-2 data, the biases do not have a strong seasonal dependence. This supports further analyses of the near-global high vertical resolution SAGE II data to quantify the seasonal cycle in the lowermost stratosphere.

Plate 4 shows monthly mean water vapor in the 320- to 360-K range (in ±5-K layers) and the 4-5 PVU bin for both hemispheres, derived from 5 years of SAGE II data (January 1986 to December 1990). This is the region of the lowermost stratosphere that is very close to but somewhat poleward of the extratropical tropopause. Since water vapor mixing ratios in the overworld (around 100 mbar or 400 K) are typically 3-6 ppmv [*Brewer*, 1949; *Hintsa et al.*, 1994], values substantially greater than 6 ppmv are evidence of transport across the extratropical tropopause. The large seasonal cycle with a maximum in the summer season clearly shows the contribution of this transport. The 10-ppmv contour in Plate 4 approximately marks the range of influence of these transport processes, which extends to near 360 K in the summer season for both hemispheres. There is a clear hemispheric asymmetry for the lower isentropes throughout the seasonal cycle, with somewhat moister air in the NH. For example, the typical summer value at 330 K is about 40 ppmv in the NH but only 25 ppmv in the SH. In the winter months the 10-ppmv contour extends to ~330 K in the NH, showing clear evidence of transport across the extratropical tropopause, while in the SH, values are below 10 ppmv for early spring over the entire potential temperature range evaluated.

To further quantify the water vapor seasonal cycle in the lowermost stratosphere, we present in Figure 2 the annual means, as well as the January and July monthly means, of water vapor for the 330-, 340-, 350-, and 360-K isentropes and the 2-7 PVU range. The January and July monthly means indicate the amplitude of the seasonal cycle. The depth of influence of STE on each isentrope can be estimated from the departure from the overworld values of 3-6 ppmv. The variation of this effect across isentropes and across PV bins is evident in this analysis. In general, both the mean and the amplitude of the seasonal cycle decrease monotonically, from low to high isentropes and from low to high PV bins. The July (January) monthly means in the NH (SH) are computed from relatively small sets of samples, which may contribute to the variability across the PV range. For the NH at 330 K the annual means are between 40 and 15 ppmv

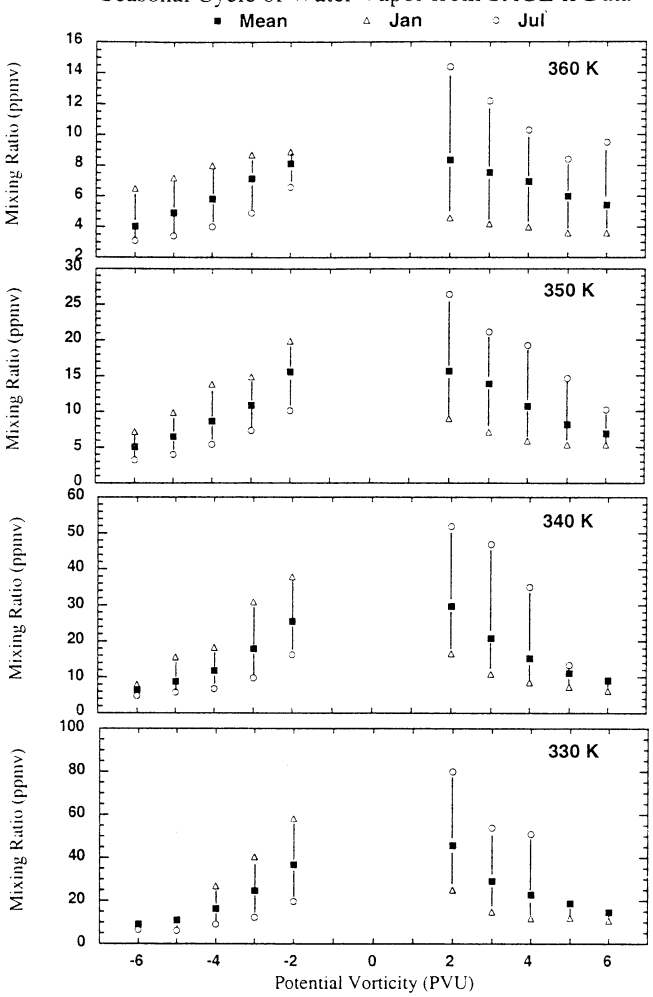

Figure 2. Annual mean, January and July monthly mean as a function of PV for 330-360 K derived from the 5-year (January 1986-December 1990) SAGE II measurements for the 2-7 PVU. The data are binned in 1-PVU intervals. PV values shown for each panel are the lower boundary of each PV bin. Note the variation of scales for the vertical coordinates, selected to best display the range of seasonal variations.

for the 2-7 PVU range. The largest seasonal cycle amplitude for this NH isentrope is ~60 ppmv. The NH 360-K result shows a significantly reduced water vapor amount and seasonal variability. The mean values on that level are from 8 to 5 ppmv, with the largest amplitude around 10 ppmv. The reduction of variability reflects the decreased effect of STE farther away from the extratropical tropopause. Both the annual and monthly means change smoothly along the PV coordinate. Again, the mean values and the amplitudes also show hemispheric asymmetries, with higher values and more pronounced seasonal cycles in the NH. For example, the 350-K seasonal cycle for the NH 3-4 PVU bin has a peak-to-peak amplitude near 15 ppmv, but it is only about half that size for the corresponding SH bin. The amplitude difference is a result of significantly wetter summers in the NH compared with the SH since the winter monthly means are nearly equal.

A combination of factors has been discussed concerning the dryness of the SH lower stratosphere in the 380- to 450-K region, as compared with the NH [*Rosenlof et al.*, 1997]. Several of

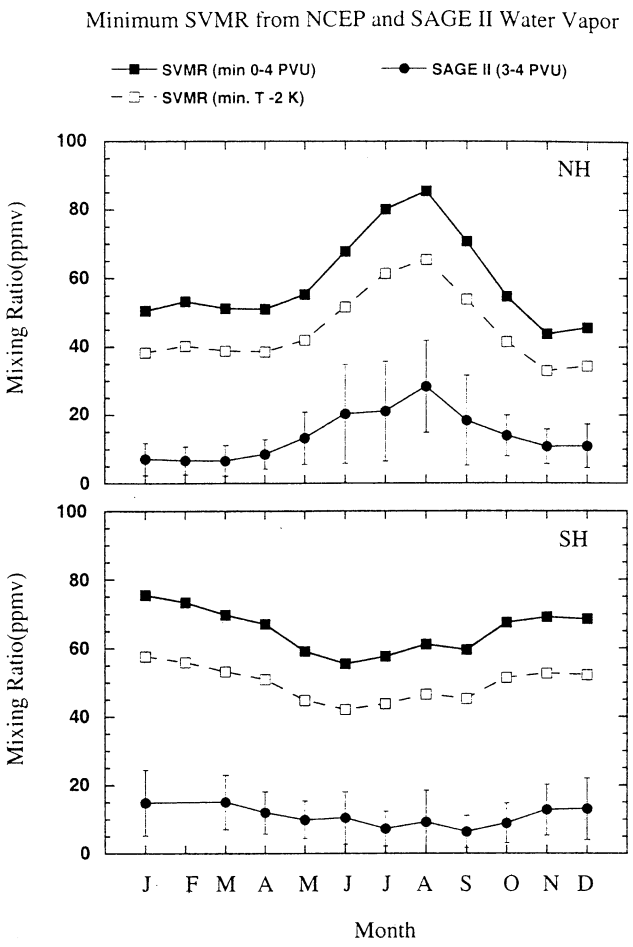

Figure 3. Seasonal cycle of minimum saturation vapor mixing ratio, derived from the NCEP temperature data, and SAGE II measurements for 3-4 PVU at 350 K. The minimum saturation vapor mixing ratio is a monthly average of the daily minimum chosen from the range of 0-4 PVU for the 350-K isentrope.

these factors also contribute to the hemispheric asymmetry in the lowermost stratosphere, the region of this analysis. The drier SH in wintertime has been discussed as an effect of lower winter temperatures [*Kelly et al.*, 1991]. Both adiabatic mixing and the convective process contribute to the transport of water vapor from the troposphere into the lowermost stratosphere. Our data analyses cannot distinguish the two processes, but the wetter NH in summer seen in the data is consistent with the stronger NH monsoon circulations, which are a major factor in the STE of water vapor [*Chen*, 1995]. It also supports the suggestion of stronger convection in the NH due to a greater landmass. The observed asymmetry with the moister NH is also consistent with a model simulation of water vapor in this altitude region [*Gettelman et al.*, 2000].

4. Saturation Vapor Mixing Ratio Derived From the NCEP Temperature Data

The thermodynamic effect of saturation over ice primarily controls the amount of water vapor entering the stratosphere via the tropical tropopause. The seasonal cycle of water vapor in the tropical lower stratosphere closely follows the seasonal cycle of the tropopause temperature [*Mote et al.*, 1996]. In contrast, it is not clear to what extent temperature controls the water vapor as it is transported into the lowermost stratosphere across the extratropical tropopause. It is more complicated to examine the water vapor-temperature relation in this region, not only because there is no climatologically well defined "cold point" along the path of quasi-horizontal transport, but also because water vapor is transported into this region via multiple pathways. Among the most important processes are downward transport from the overworld as part of the Brewer-Dobson circulation and adiabatic mixing from the troposphere along isentropes. Deep convection is an additional transport mechanism in this region. These competing processes make the signature of saturation harder to decipher.

As a first step to approaching this complex issue, we examine the relationship between saturation vapor mixing ratio (SVMR) and measured water vapor near the extratropical tropopause, using both the satellite and in situ data. In this section we present a global analysis using the SAGE II water vapor and the NCEP temperature data. Our analysis examines, on a monthly mean basis, (1) whether ice saturation sets the upper limit on water vapor near the extratropical tropopause, and (2) how well the water vapor seasonal cycles resemble the seasonal cycle of the minimum SVMR estimated for the same isentrope.

We choose 350 K to represent the isentropes in the "upper" lowermost stratosphere [*Chen*, 1995], where the exchange from the troposphere to lowermost stratosphere is largely along isentropes. It is plausible that ice saturation sets the boundary condition for the water vapor transport from the troposphere across the extratropical tropopause. Since saturation is expected to limit the water vapor amount during transport, a relevant SVMR needs to be estimated with a time interval and spatial

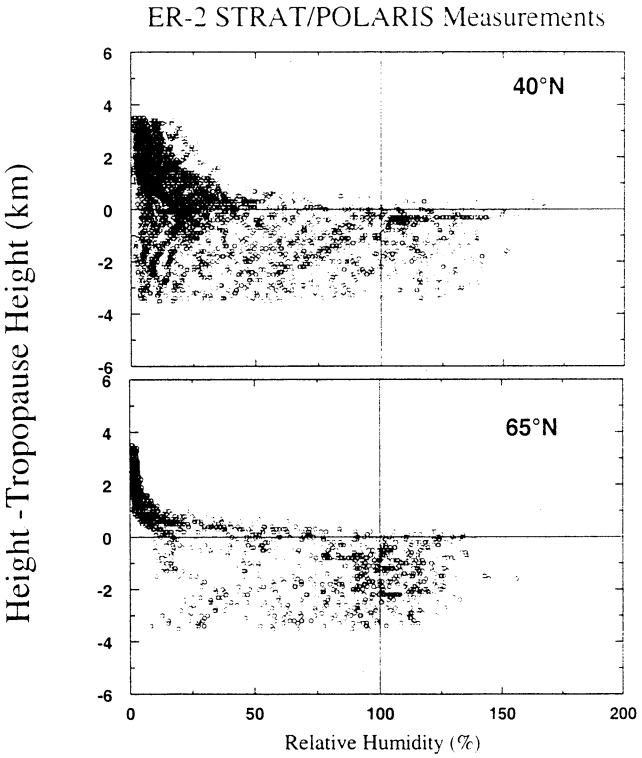

Figure 4. ER-2 measured relative humidity as a function of altitude with respect to the thermal tropopause. Data shown are within ±3.5 km of the thermal tropopause.

range that is appropriate for the timescale of the transport. It is also necessary to do so in this case because the SAGE II water vapor data are produced for clear conditions and observations made during saturation events have been excluded from the data set. We choose the spatial range to be 0-4 PVU in the PV space and use daily minimum temperature to provide a conservative estimate.

Figure 3 shows the seasonal cycles of 350-K water vapor from SAGE II measurements near the tropopause (3<PV<4) and the minimum SVMR computed from NCEP temperature data for both hemispheres. The ice saturation vapor pressure, in millibars, is calculated using the formula [*Kyle*, 1991]

$$P_s = 6.11 \times 10^{\frac{9.5T}{(265.5+T)}} \quad (1)$$

where T is temperature in Celsius. The minimum SVMR curve shows the monthly average of the daily minimum SVMR for 0-4 PVU on the 350-K isentrope. Since the relation between SVMR and temperature is exponential, a small change in temperature can produce a large change in SVMR. To take into consideration the uncertainty of the NCEP data, we also included a minimum SVMR calculated by subtracting 2 K from NCEP temperatures. The error bar for the SAGE II data indicates $\pm 1\sigma$ from the mean. Comparisons of the curves show that for both hemispheres, although the seasonal cycles, in general, are similar, the measured water vapor is much smaller than the minimum SVMR for all seasons. The average difference between the SAGE II water and the NCEP temperature based minimum SVMR is around 45 ppmv for the NH and 53 ppmv for the SH. Note that these results are relatively insensitive to the PV range in the vicinity of the tropopause; using water vapor for the 2<PV<3 PVU bin and SVMR estimated for the 0-3 PVU (not shown) gives similar results.

Figure 3 shows that the lowermost stratosphere near the extratropical tropopause is substantially undersaturated. This is consistent with the analysis of relative humidity (RH) using MLS data [*Sandor et al.*, 1998], which showed that the upper troposphere near the extratropical tropopause (although the tropopause was not identified in that analysis) is, on average, undersaturated. The RH for the 215-mbar level (near 350 K) was shown to be between 20 and 40% for the latitude range of the extratropical tropopause (20°-40°). ER-2 measurements, discussed below, also show that air parcels near the extratropical tropopause are, on average, undersaturated.

5. Saturation and Relative Humidity Derived From the ER-2 Data

During the STRAT and POLARIS missions, both water vapor and temperature were measured on board the ER-2 aircraft. We use these data to assess the issue of saturation near the tropopause. Although the coverage of these measurements is within a smaller latitude and longitude range compared with the satellite data, the higher accuracy, the finer scale of sampling, and the well colocated water vapor and temperature measurements allow a more detailed study of saturation. We use these data to derive relative humidity near the tropopause and to address the issues of how often and where saturation occurs.

The ER-2 instruments made measurements near the extratropical tropopause during ascents, descents, and "stacked" flights (horizontal flight legs at different altitudes), with the tropopause crossings occurring in two latitudinal windows, near the Arctic Circle (~64°-67°N) and near the subtropical jet (~35°-40° N). The midlatitude measurements covered all seasons, but the high latitude measurements only sampled April through July and September. We found it useful to separate the data into two groups in analyses, because different characteristics in these two latitude regions are shown in multiple trace gas profiles (L. Pan et al., manuscript in preparation, 2000).

Figure 4 shows the RH, derived using the water vapor and temperature data, as a function of height with respect to the tropopause. In this case we have used the thermal tropopause, instead of the dynamical (PV) definition of the tropopause, to be consistent with the spatial resolution of the ER-2 measurements and to use coincident temperature measurements on board the ER-2. The thermal tropopause height determination was made using the WMO definition for both ascending and descending portions of the flights. The tropopause height for the midlatitude window ranges from roughly 8 to16 km and from 7 to 12 km for the high latitude window. The average heights for the two locations are approximately 12 km (~350 K) and 10 km (~330 K), respectively.

As shown in Figure 4, relative humidity changes sharply across the tropopause in both latitude regions. Right below the tropopause, there are a significant number of supersaturation cases. To allow for measurement uncertainty, we consider values of RH between 90 and 110% to be saturated and those greater than 110% to be supersaturated. For all the measurements within 1 km below the tropopause in the midlatitude window, 10.5% are saturated and 11.4 % are super-saturated. For the high-latitude window, 28.0% and 23.0% are saturated and supersaturated, respectively. Only a small percentage of saturated cases are found to be above the tropopause, and those are all within 0.5 km of the tropopause, consistent with the uncertainty of the tropopause height determination and also consistent with the analysis of *Smith et al.* [2000]. Note that 72% of the samples measured within 1 km below the tropopause are undersaturated. Supersaturation in the upper troposphere can be understood as an effect of a nucleation barrier [*Jensen et al.*, 1998]. Our analysis of the ER-2 data finds supersaturation in 20% of the measurements, with the relative humidity as high as near 160%. This is consistent with that observed in the SUCCESS mission, where peak RH was about 150-160% [*Jensen et al.*, 1998].

To further quantify to what extent saturation sets the limit of water vapor near the tropopause, we calculate the mean and the root-mean-square of the relative humidity within a 1-km layer centered at the tropopause and binned by θ. The results for both the midlatitude and high-latitude regions, as given in Figure 5, show that although saturation does occur near the extratropical tropopause, on average, the air is undersaturated near the tropopause (with an exception at 330 K, where ER-2 measurements average 108% RH near 40°N, an interesting case that which deserves future investigation). Thus the in situ measurements support the undersaturation in this region concluded from satellite data analyses using both SAGE II (Figure 3) and MLS data [*Sandor et al.*, 1998].

6. Implications for Transport Across the Extratropical Tropopause

The amount and the seasonal cycles of water vapor in the lowermost stratosphere indicate that STE across the extratropical tropopause makes a significant contribution to this region. Using

water vapor data alone, however, it is difficult to identify the transport mechanisms (adiabatic and diabatic mixing versus convection) of this exchange and to quantify the variability of the exchange. Both the variability of mass transport across the extratropical tropopause and the water vapor content (relative humidity) of the air mass that is being transported contribute to the amount of water vapor transported. Although quantification is difficult due to these factors, it is possible to infer transport information from the global water vapor measurements using some idealized assumptions.

We consider a simple model in which the monthly mean water vapor in the lowermost stratosphere represents a balance of downward flux from the overworld and isentropic transport across the extratropical tropopause (a box with two open sides). This neglects convective transport from below the tropopause. We furthermore assume that the transport across the extratropical tropopause is at a constant rate but the water vapor content is limited by ice saturation. Under these assumptions and using q to represent the water vapor mixing ratio in this box, q_1 to represent the water vapor mixing ratio of overworld air, and q_2 for that associated with isentropic transport from the troposphere along 350 K, the fraction of air that originated from the overworld, X, can be estimated by

$$X = (q-q_2)/(q_1-q_2). \quad (2)$$

We choose the PV=3-4 PVU bin in the 350-K (i.e., Plate 2) as an example to do this estimate. To apply (2) to this PV-θ bin, we use the SAGE II 5-year PV-θ binned monthly mean mixing ratio as q and 4 ppmv as the boundary condition year-round for air from the overworld (q_1). Boundary conditions for air entering by isentropic mixing (q_2) are likely the biggest source of uncertainty in the estimate. We made estimates using two different assumptions of q_2. The first estimate assumes that this transport boundary condition is set by saturation over ice (100% RH) throughout the year and uses the minimum SVMR on the isentrope (as given in Figure 3) for q_2. The result of X, given in Figure 6, shows that under this assumption, the composition of air in this bin is primarily from the overworld for all months. The fraction varies from 70% in summer to 95% in winter for the NH and from 85% to 98% for the SH.

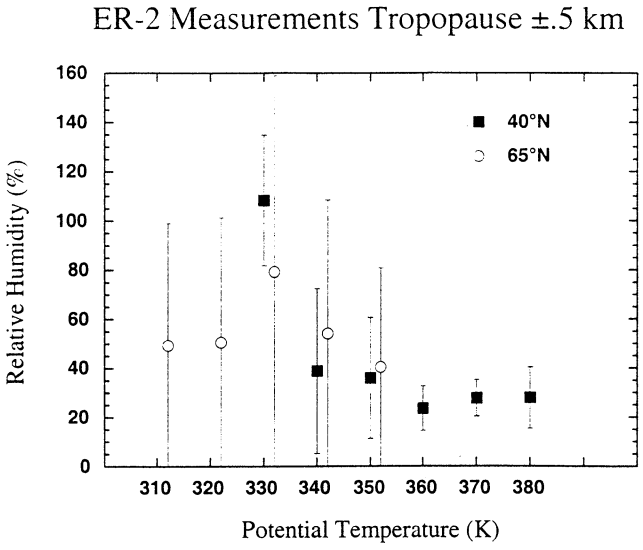

Figure 5. Mean relative humidity from the ER-2 measurements for a 1-km layer centered at the thermal tropopause as a function of potential temperature. The error bars are given by the root-mean-square deviation from the mean.

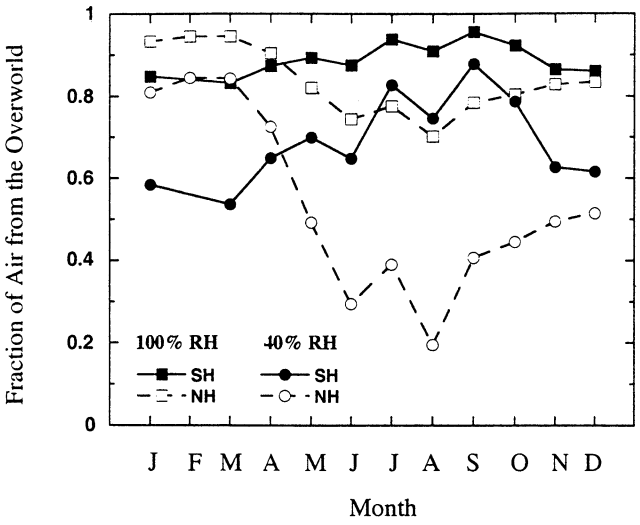

Figure 6. Seasonal cycle of the fraction of overworld contribution for the PV 3-4 bin at 350 K, for both the Northern and Southern Hemispheres, estimated using equation (2) under two sets of boundary conditions.

In general, this result likely represents an overestimate of overworld fraction, since the measurements show that the air near the extratropical tropopause is undersaturated, on average. Hence a second estimate is made using 40% RH (constant year-round) as the boundary condition for isentropic mixing across the tropopause. This value is approximately the average of ER-2 measurements near the tropopause. Our idealized model does not give information on details of small-scale transport and the origin of each air parcel; only the average condition is estimated. The fact that the boundary values may already represent a mixture of air from both sides of the tropopause does not alter the fact that this represents an average boundary condition. The result, also shown in Figure 6, gives significantly smaller fractions of overworld contribution, varying from 20% (50%) in summer to about 80% (90%) in winter for the NH (SH).

The estimate using 100% RH boundary conditions is in agreement, for the month of May, with an estimate under similar assumptions by *Dessler et al.* [1995], where the saturation temperature is derived using six water vapor profiles measured in May 1993 during the Stratospheric Photochemistry, Aerosols, and Dynamics Expedition (SPADE). We have also compared the estimates in Figure 6 with a set of estimates using balloon in situ measurements of several tracers by *Ray et al.* [1999], where different estimates were derived from three sets of NH profiles in May, June, and September. Our results using 100% and 40% RH boundary conditions bracket the *Ray et al.* [1999] results estimated from CFC-11 for NH high latitudes in June. No previous analyses for NH winter or SH are available for comparisons.

These results, although helpful as a step toward understanding the implications of the water vapor values to transport in this region, are derived under highly idealized assumptions. A more accurate transport calculation requires measurements with higher space-time resolution and accurate

three-dimensional wind analyses in this region. Analyses combining multiple tracers, in addition to water vapor and temperature, can help identify the origin of the dehydrated air in this region.

7. Summary

Both satellite and in situ measurements of water vapor in the middle world were analyzed to quantify the seasonal cycle of water vapor in the lowermost stratosphere and the effect of saturation on the amount of water vapor in this region. The seasonal cycles show that the transport of water vapor across the extratropical tropopause affects the lowermost stratosphere for the entire range of analysis (320-360 K and 2-7 PVU), particularly in the summer seasons when downward transport due to the large-scale circulation is weak. Both the annual mean and the amplitude of the seasonal cycle decrease gradually from near the tropopause to farther into the stratosphere, represented by higher PV and θ values. Both the monthly means and the seasonal cycle amplitudes are larger in the NH than in the SH.

We have also compared measured water vapor with the SVMR near the extratropical tropopause. The results from the satellite data and NCEP temperature analysis show that air in the lowermost stratosphere near the extratropical tropopause is undersaturated. Analysis of the ER-2 measurements is consistent with the satellite results, showing an average RH near the extratropical tropopause of ~40%. However, the ER-2 measurements also show a wide range of RH values in the upper troposphere, including supersaturation, with RH values up to 160% (below the tropopause). The large difference between the SVMR and measured water vapor indicates that air near the extratropical tropopause is much drier than that limited by the local temperature.

The undersaturation in this region may be a result of tropospheric circulations followed by mixing from the dry subtropical regions. Another possible mechanism for undersaturation is the outward mixing of dry air from the stratosphere due to STE in this region, which has been discussed using a model simulation [*Yang and Pierrehumbert*, 1994]. In either case our analyses support that the transport of drier air, as opposed to local saturation processes near the extratropical tropopause, limits the water vapor amount in this region.

The seasonal cycle of lowermost stratosphere water vapor is a result of STE across the extratropical tropopause and the large scale Brewer-Dobson circulation. Using the water vapor and temperature data and several assumptions, we have estimated the contribution of overworld air to the total mass in this region. The results (Figure 6) show that air in the upper part of this region (represented by the PV 3-4 bin at 350 K) is largely from the overworld and that the extratropical STE making significant contributions to the composition of this region mostly in the summer season. The large fraction of overworld air during NH winter-spring (Figure 6) is consistent with the known seasonal cycle of residual circulation, which likewise exhibits a maximum during this time [e.g., *Rosenlof*, 1995].

Acknowledgments. The authors thank Bruce Gary for providing the tropopause height analysis for the ER-2 measurements, using both MMS and MTP temperature data. We thank the members of the SAGE and MLS teams for their work in producing the SAGE II and the MLS water vapor data sets. This work is partially supported by the NASA Upper Atmosphere Research Satellite guest investigator program, the NASA Atmospheric Chemistry Modeling and Analysis Program, and the National Science Foundation through its support to the University Corporation for Atmospheric Research. E. M. Stone acknowledges the National Research Council for its NASA Resident Research Associateship award at the Jet Propulsion Laboratory, California Institute of Technology.

References

Brewer, A. W., Evidence for a world circulation provided by measurement of helium and water vapor in the stratosphere, *Q. J. R. Meteorol. Soc.*, *75*, 351-363, 1949.

Chen, P., Isentropic cross-tropopause mass exchange in the extratropics, *J. Geophys. Res.*, *100*, 16,661-16,673, 1995.

Chiou, E. W., M. P. McCormick, and W. P. Chu, Global water vapor distributions in the stratosphere and upper troposphere derived from 5.5 years of SAGE II observations (1986-1991), *J. Geophys. Res.*, *102*, 19,105-19,118, 1997.

Chu, W. P., E. W. Chiou, J. C. Larsen, L. W. Thomason, D. Rind, J. J. Buglia, S. Oltmans, M. P. McCormick, and L. M. McMaster, Algorithms and sensitivity analyses for Stratospheric Aerosol and Gas Experiment II water vapor retrieval, *J. Geophys. Res.*, *98*, 4857-4866, 1993.

Denning, R. F., S. L. Guidero, G. S. Parks, and B. L. Gary, Instrument description of the airborne microwave temperature profiler, *J. Geophys. Res.*, *94*, 16,757-16,765, 1989.

Dessler, A. E., E. J. Hintsa, E. M. Weinstock, J. G. Anderson, and K. R. Chan, Mechanisms controlling water vapor in the lower stratosphere: "A tale of two stratospheres," *J. Geophys. Res.*, *100*, 23,167-23,172, 1995.

Foot, J. S., Aircraft measurements of the humidity in the lower stratosphere from 1977 to 1980 between 45°N and 65°N, *Q. J. R. Meteorol. Soc.*, *110*, 303-319, 1984.

Gettelman, A., J. R. Holton, and A. R. Douglass, Simulations of water vapor in the lower stratosphere and upper troposphere, *J. Geophys. Res.*, *105*, 9003-9023, 2000.

Hintsa, E. J., E. M. Weinstock, A. E. Dessler, J. G. Anderson, M. Loewenstein, and J. R. Podolske, SPADE H_2O measurements and the seasonal cycle of stratospheric water vapor, *Geophys. Res. Lett.*, *21*, 2559-2562, 1994.

Hintsa, E. J., et al., Troposphere-to-stratosphere transport in the lowermost stratosphere from measurements of H_2O, CO_2, N_2O, and O_3, *Geophys. Res. Lett.*, *25*, 2655-2658, 1998.

Hintsa, E. J., E. M. Weinstock, J. G. Anderson, R. D. May, and D. F. Hurst, On the accuracy of in situ water vapor measurements in the troposphere and lower stratosphere with the Harvard Lyman-α hygrometer, *J. Geophys. Res.*, *104*, 8183-8189, 1999.

Hoerling, M. P., T. K. Schaack, and A. J. Lenzen, Global objective tropopause analysis, *Mon. Weather Rev.*, *119*, 1816-1831, 1991.

Holton, J. R., P. H. Haynes, M. E. McIntyre, A. R. Douglass, R. B. Rood, and L. Pfister, Stratosphere-troposphere exchange, *Rev. Geophys.*, *33*, 403-439, 1995.

Hoskins, B. J., Towards a PV-θ view of the general circulation, *Tellus, 43AB*, 27-35, 1991.

Jensen, E. J., et al., Ice nucleation processes in upper tropospheric wave-clouds observed during SUCCESS, *Geophys. Res. Lett.*, *25*, 1363-1366, 1998.

Kelly, K. K., A. F. Tuck, and T. Davis, Wintertime asymmetry of upper tropospheric water between the Northern and Southern Hemispheres, *Nature*, *353* 244-247, 1991.

Kyle, T. G., *Atmospheric Transmission, Emission and Scattering*, p. 9, Pergamon, Tarrytown, N.Y., 1991.

McCormick, M. P., SAGE II: An overview, *Adv. Space Res.*, *7*, 219-226, 1987.

McCormick, M. P., E. W. Chiou, L. R. McMaster, W. P. Chu, J. C. Larsen, D. Rind, and S. Oltmans, Annual variations of water vapor in the stratosphere and upper troposphere observed by the Stratospheric Aerosol and Gas Experiment II, *J. Geophys. Res.*, *98*, 4867-4874, 1993.

Mote, P. W., K. H. Rosenlof, M. E. McIntyre, E. S. Carr, J. C. Gille, J. R. Holton, J. S. Kinnersley, H. C. Pumphrey, J. M. Russell, and J. W. Waters, An atmospheric tape recorder: The imprint of tropical tropopause temperatures on stratospheric water vapor, *J. Geophys. Res.*, *101*, 3989-4006, 1996.

Pan, L., S. Solomon, W. J. Randel, J. F. Lamarque, P. Hess, J. C. Gille, E.W. Chiou, and M. P. McCormick, Hemispheric asymmetries and

seasonal variations of the lowermost stratospheric water vapor and ozone derived from SAGE II data, *J. Geophys. Res.*, *102*, 28,177-28,184, 1997.

Ray, E. A., F. L. Moore, J. W. Elkins, G. S. Dutton, D. W. Fahey, H. Vomel, S. J. Oltmans, and K. H. Rosenlof, Transport into the Northern Hemisphere lowermost stratosphere revealed by in situ tracer measurements, *J. Geophys. Res.*, *104*, 26,565-26,580, 1999.

Rind, D., E. W. Chiou, W. P. Chu, S. Oltmans, J. Lerner, J. Larsen, M. P. McCormick, and L. R. McMaster, Overview of the Stratospheric Aerosol and Gas Experiment II water vapor observations: Method, validation, and data characteristics, *J. Geophys. Res.*, *98*, 4835-4856, 1993.

Rosenlof, K. H., Seasonal cycle of the residual mean meridional circulation in the stratosphere, *J. Geophys. Res.*, *100*, 5173-5191, 1995.

Rosenlof, K. H., A. F. Tuck, K. K. Kelly, J.M. Russell, and M.P. McCormick, Hemispheric asymmetries in water vapor and influences about transport in the lower stratosphere, *J. Geophys. Res.*, *102*, 13,213-13,234, 1997.

Sandor, B. J., W. G. Read, J. W. Waters, and K. H. Rosenlof, Seasonal behavior of tropical to midlatitude upper troposphere water vapor from UARS MLS, *J. Geophys. Res.*, *103*, 25,935-25,947, 1998.

Scott, S. G., T. P. Bui, K. R. Chan, and S. W. Bowen, The Meteorological Measurement System on the NASA ER-2 aircraft, *J. Atmos. Oceanic Technol.*, *7*, 525-540, 1990.

Smith, J. B., E. J. Hintsa, N. T. Allen, R. M. Stimpfle, and J. G. Anderson, Mechanisms for mid-latitude ozone loss: Heterogeneous chemistry in the lowermost stratosphere?in press, *J. Geophys. Res.*, 2000.

Stone, E. M., L. Pan, B. J. Sandor, W. G. Read, and J. W. Waters, Spatial distributions of upper tropospheric water vapor measurements from the UARS Microwave Limb Sounder, *J. Geophys. Res.*, *105*, 12,149-12,161, 2000.

Waters, J. W., *Microwave Limb Sounding: Atmospheric Remote Sensing by Microwave Radiometry*, edited by M. A. Janssen, pp. 383-496, John Wiley, New York, 1993.

Weinstock, E. M., E. J. Hintsa, A. E. Dessler, J. F. Oliver, N. L. Hazen, J. N. Demusz, N. T. Allen, L. B. Lapson, and J. G. Anderson, New fast response photofragment fluorescence hygrometer for use on the NASA ER-2 and the Perseus remotely piloted aircraft, *Rev. Sci. Instrum.*, *65*, 3544-3554, 1994.

Yang, H., and R. T. Pierrehumbert, Production of dry air by isentropic mixing, *J. Atmos. Sci.*, *51*, 3437-3454, 1994.

E. J. Hintsa, Department of Marine Chemistry and Geochemistry, Woods Hole Oceanographic Institution, Woods Hole, MA 025430-1541.

L. L. Pan and W. J. Randel, National Center for Atmospheric Research, P. O. Box 3000, Boulder, CO 80307-3000. (liwen@ucar.edu)

E. M. Stone, Bay Area Environmental Research Institute, NASA Ames Research Center, Moffett Field, CA 94035.

E. M. Weinstock, Department of Chemistry and Biological Chemistry, Harvard University, Cambridge, MA 02138.

(Received November 17, 1999; revised June 8, 2000;
accepted June 15, 2000.)